

## Spectroscopic studies and crystal-field analysis of $\text{Cm}^{3+}$ and $\text{Gd}^{3+}$ in $\text{LuPO}_4$

J. Sytsma, K. M. Murdoch, and N. M. Edelstein

*Chemical Sciences Division, Lawrence Berkeley Laboratory, Berkeley, California 94720*

L. A. Boatner and M. M. Abraham

*Solid State Division, Oak Ridge National Laboratory, Oak Ridge, Tennessee 37831*

(Received 10 April 1995)

Optical-absorption and laser-selective-excitation spectroscopy have been used to investigate the electronic energy level structures of the actinide ion  $\text{Cm}^{3+}$  and the lanthanide ion  $\text{Gd}^{3+}$  in host crystals of  $\text{LuPO}_4$ . Crystal-field levels have been determined up to 35 000 and 37 000  $\text{cm}^{-1}$ , respectively, for the principal  $D_{2d}$  symmetry substitutional site. These have been analyzed in terms of a parametric Hamiltonian and the two systems compared. High-resolution fluorescence spectroscopy was used to resolve the ground-term splittings of  $\text{Cm}^{3+}$  and these are compared to the zero-field splittings measured in a previous EPR investigation. Some weaker fluorescence features also were observed, which are attributed to minor  $\text{Cm}^{3+}$  sites in the host lattice. Two-photon excitation was observed to the  ${}^6P_{5/2}$  and  ${}^6P_{7/2}$  multiplets of  $\text{Gd}^{3+}$ .

### INTRODUCTION

Mixed-lanthanide orthophosphates exist in nature as the monoclinic mineral monazite. In the form of pure lanthanide orthophosphates (i.e.,  $\text{LPO}_4$ , where  $L=\text{La, Ce, . . . , Yb, Lu}$ ), however, these compounds crystallize in two different structural types. For those ions in the series extending from La to Gd, the orthophosphates exist in the stable high-temperature, monoclinic monazite structure, while orthophosphates for the ions extending from Tb to Lu crystallize in the stable tetragonal xenotime structure at high temperatures.<sup>1,2</sup>

The lanthanide orthophosphates are characterized by an unusual combination of favorable chemical and physical properties which, during the period of approximately 1979 to 1989, led to their consideration and in-depth characterization as a potential advanced-ceramic medium for the encapsulation and permanent disposal of high-level radioactive wastes.<sup>3-10</sup> The actinides plutonium, americium, and curium have been reported to form orthophosphates that also have the monoclinic monazite structure.<sup>11,12</sup> This property is not only pertinent to the possible use of lanthanide orthophosphate ceramics as nuclear waste forms, but has led also to recent suggestions concerning the applicability of mixed lanthanide/actinide orthophosphates as materials for securing fissile isotopes subsequent to the deactivation of nuclear warheads. Interest in the optical, magnetic, structural, and electronic properties of lanthanide orthophosphates has also been stimulated recently by the potential of these very stable and radiation-damage-resistant materials as thermophosphors for remote-temperature measurements, as x- and  $\gamma$ -ray scintillators for medical-imaging applications, and as laser hosts.<sup>13,14</sup>

In addition to the potential applications of the lanthanide orthophosphates noted above, the diamagnetic tetragonal-symmetry end member of the transition series,  $\text{LuPO}_4$ , plus the related diamagnetic phosphates  $\text{YPO}_4$  and  $\text{ScPO}_4$  have proven to be ideal hosts for the incorporation of dilute impurities representing a wide variety of rare-earth, actinide, and iron-group ions for the purpose of carrying out fundamental spectroscopic investigations. Such basic studies have

included experiments employing optical,<sup>15-17</sup> electron-paramagnetic-resonance (EPR),<sup>18,19</sup> neutron,<sup>20,21</sup> and electronic Raman<sup>22,23</sup> spectroscopies.

In the present work,  $\text{LuPO}_4$  has been utilized as a host for the incorporation of the trivalent actinide ion  $\text{Cm}^{3+}$ . This system has previously been the subject of several EPR investigations,<sup>24</sup> and complimentary high-resolution Zeeman data have also been obtained<sup>25</sup> that confirmed the EPR-based assignment of the crystal-field ground state. Most recently, the zero-field splittings of the ground term of  $\text{Cm}^{3+}$  have been determined from a detailed analysis of the anisotropic EPR results, and a number of absorption and emission lines have been reported for this system up to 25 000  $\text{cm}^{-1}$ .<sup>26</sup> Here we report absorption measurements for  $\text{Cm}^{3+}/\text{LuPO}_4$  up to  $\sim 37\,000\text{ cm}^{-1}$ , as well as excitation spectra for the  $4f^7$  analog  $\text{Gd}^{3+}$  in  $\text{LuPO}_4$ , and analyze these results in terms of a parametric Hamiltonian. High-resolution fluorescence measurements have been used to resolve the ground-term splitting of  $\text{Cm}^{3+}$  and have also revealed the existence of several other low-concentration  $\text{Cm}^{3+}$  sites in  $\text{LuPO}_4$ . Finally, the present results are compared with the values of the zero-field splittings obtained from EPR measurements.<sup>26</sup>

### EXPERIMENTAL

Single crystals of  $\text{LuPO}_4$  doped with either  $\text{Cm}^{3+}$  (using the  ${}^{248}\text{Cm}$  isotope with a half-life of  $3.4 \times 10^5$  y) or  $\text{Gd}^{3+}$  were grown using a high-temperature solution technique described previously.<sup>27,28</sup> The  $\text{Gd}^{3+}/\text{LuPO}_4$  single-crystal dimensions were typically  $0.5 \times 4.0 \times 10.0\text{ mm}^3$ . The  $\text{Cm}^{3+}$ -doped  $\text{LuPO}_4$  single-crystal specimen, however, was relatively small with dimensions of approximately  $0.5 \times 2.0 \times 1.0\text{ mm}^3$ . The  $\text{Gd}^{3+}$ -doped samples were grown with 0.1 mol %  $\text{Gd}_2\text{O}_3$  added to the starting composition relative to lutetium oxide, but the actual concentration of  $\text{Gd}^{3+}$  present in the as-grown crystal was not quantitatively determined. The amount of  $\text{Cm}^{3+}$  present in the as-grown  $\text{Cm}^{3+}/\text{LuPO}_4$  crystal was also not determined by quantitative analysis, but is estimated to be less than 0.1 mol %.

Spectroscopic measurements were carried out using crystals that were selected on the basis of their optical quality, with the samples either cooled to liquid-helium temperature or at room temperature. In the case of the low-temperature investigations, the doped crystals were cooled to 4.2 K using an Oxford Instruments model CF 1204 optical cryostat. In the case of  $\text{Cm}^{3+}$  in  $\text{LuPO}_4$ , the energy-level structure was established primarily using optical-absorption methods. The radioactive  $\text{Cm}^{3+}$  sample was sealed in a quartz ampoule under a partial pressure of helium for containment purposes, and the room-temperature measurements on this material were also carried out inside the cryostat as a means of achieving secondary containment for the radioactive specimen. In carrying out the single-photon, high-resolution absorption measurements, two different lamps were utilized: a 100 W quartz lamp for the spectral region of 16 000–25 000  $\text{cm}^{-1}$  and a 75 W Xe lamp (in an Oriel Photomax housing) for the spectral region 25 000–35 000  $\text{cm}^{-1}$ . Prior to being focused on the sample by a lens with a focal length of 10 cm, the incident light passed through a water filter in order to reduce the amount of infrared radiation incident on the crystal. The transmitted light was collected by a 10 cm focal length collimating lens, focused on the entrance slit of a Spex 1403 double monochromator, and was subsequently detected using a cooled Hamamatsu R375 photo multiplier (PMT). The typical slit width was 100  $\mu\text{m}$ , which yielded a resolution of  $\sim 1 \text{ cm}^{-1}$ . Since the monochromator does not operate in the first-order mode above 30 500  $\text{cm}^{-1}$ , the instrument was used in the second order for energies above this value. An additional Corning 7-54 color filter was used to stop the visible portion of the lamp spectrum. The monochromator was calibrated throughout the region investigated by employing a number of calibration lamps.

Laser-selective excitation was used to determine the positions of the  $\text{Gd}^{3+}$  energy levels, since the single-crystal specimens were too thin to produce appreciable absorption. In this case, the single-photon excitation spectra were obtained using a PDL-3 dye laser that was pumped by a DCR-3A Nd-YAG laser—both from Spectra Physics. The output of the dye laser was frequency doubled using a Spectra Physics WEX-1 wavelength extender. This system was used to scan the spectral region of the  $^8S_{7/2}$  to  $^6P_{7/2}$ ,  $^6P_{5/2}$ ,  $^6P_{3/2}$ , and  $^6I_J$  transitions (i.e., 32 000–37 000  $\text{cm}^{-1}$ ). To cover the region from 29 900 to 32 800  $\text{cm}^{-1}$ , the second harmonic of the Nd-YAG laser was used to pump a solution of DCM dye dissolved in methanol. Rhodamine 640 and Fluorescein 548 dyes were used for the spectral regions from 32 200 to 33 400  $\text{cm}^{-1}$  and 35 000 to 37 000  $\text{cm}^{-1}$ , respectively. Wavelength calibration of the dye laser was verified using the double monochromator for several wavelengths within the tuning curve of each dye.

The excitation signals were detected by monitoring the overall  $\text{Gd}^{3+}$  emission. All the  $\text{Gd}^{3+}$  fluorescence was from the  $^6P_{7/2} \rightarrow ^8S_{7/2}$  transition. This luminescence was detected using a Hamamatsu IP28 PMT which was located at an angle of  $90^\circ$  relative to the incident laser beam. The entrance of the PMT was covered with a 310 nm line filter [full width at half maximum (FWHM) 5 nm] to reduce the detection of scattered laser light. In order to determine the positions of the crystal-field components of the emitting level ( $^6P_{7/2}$ ), a two-photon excitation spectrum was obtained by removing the

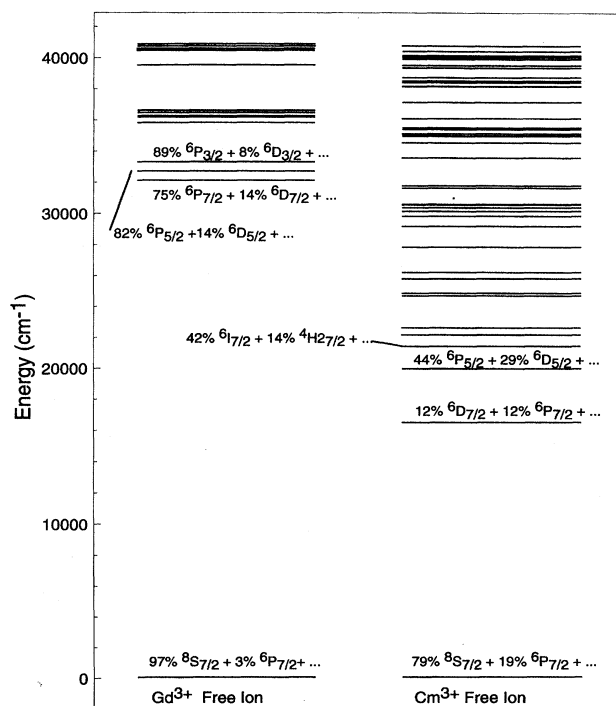


FIG. 1. Energy-level diagram comparing the free-ion energy levels of the  $f^7$  ions  $\text{Gd}^{3+}$  and  $\text{Cm}^{3+}$ .

frequency-doubling crystals in the wavelength extender. The PMT output was directed into a SR400 photon counter (Stanford Research Systems) which was triggered by the current pulses from a photodiode monitoring a residual signal from the second harmonic of the Nd-YAG laser. In order to discriminate the signal from scattered laser light, a gate delay of 1 ms was used for the photon counter. The gate width was set to 30 ms. The photon counter integrated the counts over, typically, ten laser pulses, after which the total number of counts was read and averaged by the computer. No significant difference was observed between the  $\text{Gd}^{3+}$  spectra obtained at room temperature versus liquid-helium temperature. The absorption measurements for the  $\text{Cm}^{3+}/\text{LuPO}_4$  case, however, yielded different results for the two temperatures due to the significantly larger splitting of the  $\text{Cm}^{3+}$  ground state, which is only partially  $^8S_{7/2}$  in character. The energy values reported here are those determined at liquid-helium temperature.

## THEORY

The trivalent ions  $\text{Cm}^{3+}$  and  $\text{Gd}^{3+}$  are characterized by  $5f^7$  and  $4f^7$  electronic configurations, respectively. The corresponding major differences between the properties of these two ions are reduced values of the electrostatic interaction and significantly larger spin-orbit-coupling parameters for the actinide ions, and an increased radial extension of the  $5f$  orbitals as compared with the  $4f$  orbitals resulting in a much larger crystal-field interaction in the actinide case. Intermediate-coupling effects are much more pronounced for the  $\text{Cm}^{3+}$  ion. This can be seen from Fig. 1 where the energy

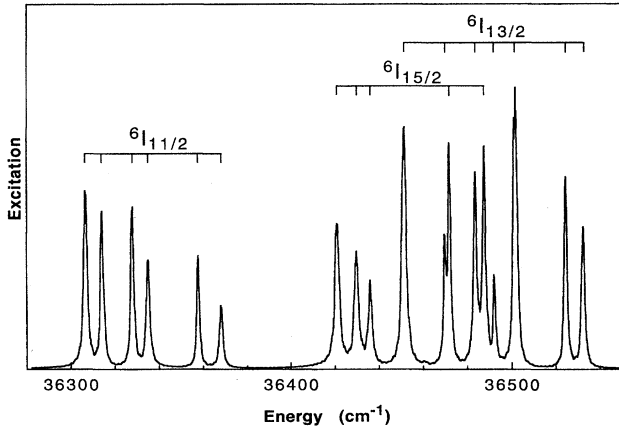


FIG. 2. A single-photon excitation spectrum for  $\text{Gd}^{3+}$  incorporated as a dilute impurity in  $\text{LuPO}_4$ .

levels of the  $\text{Gd}^{3+}$  and  $\text{Cm}^{3+}$  free ions are compared. As a consequence of the almost 100%  $^8S_{7/2}$  character of the ground term of the  $\text{Gd}^{3+}$  ion, the corresponding crystal-field splittings are on the order of  $1 \text{ cm}^{-1}$  (a pure  $S$  state is spherically symmetric and is not split by a crystalline-electric field to first order). However, the ground term wave function of the  $\text{Cm}^{3+}$  ion is of  $\sim 80\%$   $^8S_{7/2}$  character due to relatively large intermediate-coupling effects that result in an admixture of other states with the same value of  $J$ , but with different values of  $L$  and  $S$ . Thus the  $\text{Cm}^{3+}$  ground-state splittings are on the order of  $5\text{--}50 \text{ cm}^{-1}$ , depending on the strength of the crystal field associated with a given host lattice. In the case of trivalent curium in single crystals of  $\text{LuPO}_4$ , these ground-state splittings have been measured using EPR spectroscopy.<sup>26</sup>

In the present investigation, the  $\text{LuPO}_4$  host lattice is characterized by the tetragonal zircon-type structure with space group  $D_{4h}$  and  $D_{2d}$  symmetry at the metal-cation site, where  $\text{Gd}^{3+}$  or  $\text{Cm}^{3+}$  enter the lattice substitutionally for  $\text{Lu}^{3+}$ . The  $J$  states of the substitutional ions will be split by the crystal field into two types of Kramers doublets with  $D_{2d}$ -symmetry labels,  $\Gamma_6$  or  $\Gamma_7$ . The selection rules for electric-dipole transitions between such doublets are<sup>29</sup>

$$\Gamma_6, \Gamma_7 \leftrightarrow \Gamma_6, \Gamma_7: \quad \sigma \text{ polarization,}$$

$$\Gamma_6 \leftrightarrow \Gamma_7: \quad \pi \text{ polarization.}$$

The observed energy levels were fitted to a phenomenological Hamiltonian  $H = H_{\text{FI}} + H_{\text{CF}}$  by a simultaneous diagonalization of the free-ion Hamiltonian  $H_{\text{FI}}$  and the crystal-field Hamiltonian  $H_{\text{CF}}$ . The free-ion Hamiltonian is given by the expression<sup>30,31</sup>

$$\begin{aligned} H_{\text{FI}} = & \sum_{k=0,2,4,6} F^k(nf, nf) f_k + \zeta_f \alpha_{\text{SO}} + \alpha L(L+1) + \beta G(G_2) \\ & + \gamma(R_7) + \sum_{k=2,3,4,6,7,8} T^k t_k + \sum_{k=0,2,4} M^k m_k \\ & + \sum_{k=2,4,6} P^k p_k, \end{aligned} \quad (1)$$

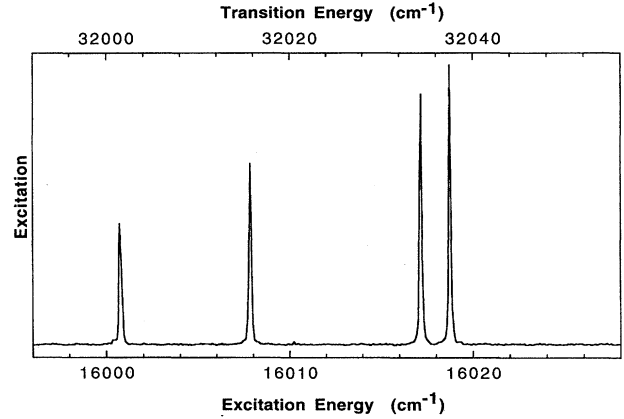


FIG. 3. A two-photon excitation spectrum showing the  $^6P_{7/2}$  excitation energies for  $\text{Gd}^{3+}$  incorporated as a dilute impurity in  $\text{LuPO}_4$ .

where  $F^k(nf, nf)$ 's and  $\zeta_f$  represent the radial parts of the electrostatic and spin-orbit interaction, respectively, between  $f$  electrons, and  $f_k$  and  $\alpha_{\text{SO}}$  are the angular parts of these interactions. The parameters  $\alpha$ ,  $\beta$ , and  $\gamma$  are associated with the two-body effective operators of the configuration interaction and the  $T^k$ 's are the corresponding parameters for the three-body-configuration interaction. The  $M^k$  parameters arise from spin-spin and spin-other-orbit interactions and the  $P^k$  parameters represent the electrostatic-spin-orbit interaction with higher configurations. The  $T^k$ ,  $M^k$ , and  $P^k$  are the radial parts of the interactions, whereas  $t_k$ ,  $m_k$ , and  $p_k$  are the corresponding angular parts. For the different interaction mechanisms present the angular parts can be evaluated exactly, while the radial portions are treated as parameters.

For  $D_{2d}$  symmetry, the crystal-field Hamiltonian can be expressed in terms of five phenomenological parameters  $B_q^k$  and the angular tensor operators  $C_q^k$ . For this particular symmetry, the values of  $|q|$  are limited to 0 and 4 and the Hamiltonian is given by<sup>31</sup>

$$\begin{aligned} H_{\text{CF}} = & B_0^2 C_0^2 + B_0^4 C_0^4 + B_4^4 [C_{-4}^4 + C_4^4] \\ & + B_0^6 C_0^6 + B_4^6 [C_{-4}^6 + C_4^6]. \end{aligned} \quad (2)$$

The quality of the fits to the above expressions were determined in two different ways. First, the deviation  $\sigma$  (in  $\text{cm}^{-1}$ ) is calculated using

$$\sigma = \sum \left[ \frac{(E_{\text{exp}} - E_{\text{calc}})^2}{(n-p)} \right]^{1/2}, \quad (3)$$

where  $n$  is equal to the number of levels and  $p$  is the number of parameters that are varied freely. For fits to the lanthanide ions' energy-level structure, this value is generally on the order of  $10\text{--}15 \text{ cm}^{-1}$ . For the actinides, however,  $\sigma$  is larger. Second, the  $g$  values of the levels can be calculated from the wave functions obtained by the diagonalization of the Hamiltonian matrix. To compare the magnitudes of the crystal fields for the  $\text{Gd}^{3+}$  and the  $\text{Cm}^{3+}$  ions, the quantity

TABLE I. Parameter values for  $Gd^{3+}$  and  $Cm^{3+}$  (A site) diluted in  $LuPO_4$ . Values in square brackets were fixed during the fitting procedure. Errors in parameter values given in parentheses.

Parameter ( $cm^{-1}$ )	$Cm^{3+}$ <sup>a</sup>	$Gd^{3+}$ <sup>b</sup>
$F^2$	84 075.0(84.8)	54 669.1(102.0)
$F^4$	61 410.8(105.6)	44 759.8(163.1)
$F^6$	44 425.9(62.7)	33 021.4(108.8)
$\zeta$	1 494.0(9.8)	2 867.7(15.5)
$\alpha$	[18.92]	30.27(7.9)
$\beta$	[-600.0]	-981.6(85.2)
$\gamma$	[1575.0]	749.3(105.5)
$T^2$	[300.0]	[200.0]
$T^3$	[42.0]	[50.0]
$T^4$	[62.0]	[40.0]
$T^6$	[-295.0]	[-360.0]
$T^7$	[350.0]	[390.0]
$T^8$	[310.0]	(340.0)
$M^0$	[3.22]	[1.09]
$M^2$	[1.80]	[0.610]
$M^4$	[1.22]	[0.414]
$P^2$	[676.0]	[912.0]
$P^4$	[507.0]	[684.0]
$P^6$	[338.0]	[456.0]
$B_0^2$	168.6(39.8)	442.7(49.7)
$B_0^4$	220.1(80.4)	304.1(66.9)
$B_4^4$	-1 034.2(54.0)	-1 980.3(54.6)
$B_0^6$	-733.4(82.5)	-2 880.1(64.6)
$B_4^6$	960.6(69.5)	881.3(63.5)
$N'_v$	657.4	1 295.6

<sup>a</sup>44 levels,  $\sigma = 15.5 \text{ cm}^{-1}$ .

<sup>b</sup>60 levels,  $\sigma = 30.8 \text{ cm}^{-1}$ .

$N'_v$ , which is linearly related to the scalar crystal-field strength parameter  $N_v$  defined by Auzel and Malta,<sup>32</sup> is used:

$$N'_v = \frac{N_v}{4\pi} = \left[ \sum_{k,q} \frac{(B_q^k)^2}{(2k+1)} \right]^{1/2}. \quad (4)$$

This parameter allows a comparison to be made between the magnitudes of the crystal fields for different  $f^N$  ions in the same host and a particular  $f^N$  ion in different hosts.

## RESULTS

### A. Excitation spectra of $Gd^{3+}$ in $LuPO_4$

Most of the levels anticipated in the region from 32 000 to 37 000  $cm^{-1}$  were, in fact, observed experimentally. In this region the  ${}^6P_J$  states [ $J=7/2, 5/2, 3/2$ ] and the  ${}^6I_J$  states [ $J=7/2, 9/2, 11/2, 13/2, 15/2, 17/2$ ] are expected. The crystal field removes all degeneracies (except for the Kramers degeneracy) and thus 48 levels are expected. Figure 2 shows a typical spectrum. The lines are extremely narrow, with a full width at half maximum (FWHM) peak intensity of less than 1  $cm^{-1}$  at room temperature and 0.5  $cm^{-1}$  at liquid-helium temperature. A total of 45 lines was observed.

Two-photon excitation was utilized in order to measure the energies of the  ${}^6P_{7/2}$  and  ${}^6P_{5/2}$  multiplets at room and

TABLE II. Calculated and experimental energy levels for  $Gd^{3+}/LuPO_4$ . The numbers before the  $\Gamma_6$  and  $\Gamma_7$  labels in the first column are used to define a particular level and start from the lowest energy level of that irreducible representation.

Level	Largest ${}^sL_J$ comp.	Calc. energy ( $cm^{-1}$ )	Expt. energy ( $cm^{-1}$ )	$E_{exp} - E_{calc}$ ( $cm^{-1}$ )
$1\Gamma_7$	${}^8S_{7/2}$	-0.51	0.0	0.51
$1\Gamma_6$	${}^8S_{7/2}$	-0.42		
$2\Gamma_6$	${}^8S_{7/2}$	-0.35		
$2\Gamma_7$	${}^8S_{7/2}$	-0.31		
$3\Gamma_7$	${}^6P_{7/2}$	32 010.8	32 001.1	-9.7
$3\Gamma_6$	${}^6P_{7/2}$	32 023.4	32 015.1	-8.3
$4\Gamma_6$	${}^6P_{7/2}$	32 049.2	32 033.7	-15.5
$4\Gamma_7$	${}^6P_{7/2}$	32 051.7	32 036.9	-14.8
$5\Gamma_6$	${}^6P_{5/2}$	32 592.1	32 600.4	8.3
$6\Gamma_6$	${}^6P_{5/2}$	32 609.8		
$5\Gamma_7$	${}^6P_{5/2}$	32 611.2	32 621.3	10.1
$6\Gamma_7$	${}^6P_{3/2}$	33 172.3	33 182.5	10.2
$7\Gamma_6$	${}^6P_{3/2}$	33 181.0	33 196.9	15.8
$7\Gamma_7$	${}^6I_{7/2}$	35 669.6	35 674.9	5.3
$8\Gamma_6$	${}^6I_{7/2}$	35 674.4	35 685.6	11.2
$8\Gamma_7$	${}^6I_{7/2}$	35 719.6	35 732.6	13.0
$9\Gamma_6$	${}^6I_{7/2}$	35 721.8	35 735.9	14.1
$9\Gamma_7$	${}^6I_{9/2}$	36 010.8	36 028.0	17.2
$10\Gamma_6$	${}^6I_{9/2}$	36 021.3	36 036.9	15.6
$10\Gamma_7$	${}^6I_{9/2}$	36 037.2	36 051.4	14.2
$11\Gamma_6$	${}^6I_{9/2}$	36 066.5	36 073.7	7.2
$11\Gamma_7$	${}^6I_{9/2}$	36 068.7	36 084.5	15.8
$12\Gamma_7$	${}^6I_{17/2}$	36 126.4	36 097.2	-29.2
$13\Gamma_7$	${}^6I_{17/2}$	36 129.0	36 101.8	-27.1
$12\Gamma_6$	${}^6I_{17/2}$	36 129.2	36 106.7	-22.5
$14\Gamma_7$	${}^6I_{17/2}$	36 134.9	36 110.1	-24.8
$13\Gamma_6$	${}^6I_{17/2}$	36 136.6	36 115.4	-21.2
$15\Gamma_7$	${}^6I_{17/2}$	36 139.9		
$14\Gamma_6$	${}^6I_{17/2}$	36 143.1	36 119.4	-23.7
$16\Gamma_7$	${}^6I_{17/2}$	36 145.1	36 123.3	-21.8
$15\Gamma_6$	${}^6I_{17/2}$	36 146.1	36 141.5	-4.6
$17\Gamma_7$	${}^6I_{11/2}$	36 289.1	36 306.5	17.4
$16\Gamma_6$	${}^6I_{11/2}$	36 298.1	36 313.8	15.7
$18\Gamma_7$	${}^6I_{11/2}$	36 317.9	36 327.6	9.7
$17\Gamma_6$	${}^6I_{11/2}$	36 320.7	36 334.6	13.9
$19\Gamma_7$	${}^6I_{11/2}$	36 348.9	36 357.1	8.2
$18\Gamma_6$	${}^6I_{11/2}$	36 355.8	36 367.4	11.6
$19\Gamma_6$	${}^6I_{15/2}$	36 426.0	36 420.0	-6.0
$20\Gamma_7$	${}^6I_{15/2}$	36 433.3	36 428.9	-4.4
$20\Gamma_6$	${}^6I_{15/2}$	36 442.1	36 435.0	-7.1
$21\Gamma_7$	${}^6I_{15/2}$	36 448.9		
$22\Gamma_7$	${}^6I_{13/2}$	36 450.3	36 450.6	0.3
$21\Gamma_6$	${}^6I_{13/2}$	36 455.6		
$23\Gamma_7$	${}^6I_{15/2}$	36 466.5		
$22\Gamma_6$	${}^6I_{13/2}$	36 468.9	36 468.8	-0.1
$23\Gamma_6$	${}^6I_{15/2}$	36 472.4	36 470.7	-1.7
$24\Gamma_7$	${}^6I_{13/2}$	36 481.3	36 482.4	1.1
$24\Gamma_6$	${}^6I_{15/2}$	36 487.8	36 486.5	-1.3
$25\Gamma_6$	${}^6I_{13/2}$	36 494.2	36 490.8	-3.4
$25\Gamma_7$	${}^6I_{15/2}$	36 502.1	36 500.9	-1.2
$26\Gamma_7$	${}^6I_{13/2}$	36 517.8	36 523.2	5.4
$26\Gamma_6$	${}^6I_{13/2}$	36 524.5	36 531.2	6.7

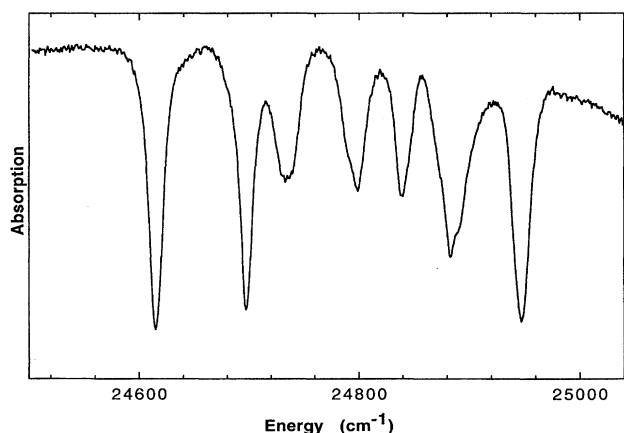


FIG. 4. An optical-absorption spectrum showing the nominally  $^8S_{7/2}$  to  $^6I_{7/2}$  transitions for  $\text{Cm}^{3+}$  incorporated as a dilute impurity in  $\text{LuPO}_4$ .

liquid-helium temperatures. Figure 3 shows a two-photon excitation spectrum at helium temperature. All four crystal-field levels were observed for the  $^6P_{7/2}$  multiplet but only two of three crystal-field levels were found for the  $^6P_{5/2}$  multiplet. The relative crystal-field splittings for the excited  $^6P_{7/2}$  multiplet as a function of temperature are unusual: room temperature—0.0, 16.1, 35.6, and 39.5  $\text{cm}^{-1}$ ; helium temperature—0.0, 14.0, 32.6, and 35.8  $\text{cm}^{-1}$ . All other levels were found by one-photon excitation.

In order to fit the levels to the Hamiltonians of Eqs. (1) and (2), the free-ion parameters for  $\text{Gd}^{3+}$  in  $\text{LaF}_3$  as determined by Carnall *et al.*<sup>33</sup> were used, and the levels assigned up to  $^6I_{9/2}$ . Initially, only the crystal-field parameters and the spin-orbit coupling parameter were allowed to vary. All other parameters were fixed at the values found for  $\text{Gd}^{3+}$  in  $\text{LaF}_3$ . The suite of programs *f-Shell Empirical Programs* written by Dr. M. F. Reid (University of Canterbury, Christchurch, New Zealand) were used for all calculations. It is assumed that the configuration interaction parameters will not change significantly from crystal to crystal. After fitting, the original assignments were compared with the calculated assignments and, if necessary, changes in the original assignments were made. Based on these initial calculations, additional levels could be assigned as well. This process was repeated until all of the observed levels were assigned. The free-ion parameters  $F^k$  ( $k=2,4,6$ ) were then varied simultaneously with the crystal-field parameters and  $\zeta_f$ . The "final fit" parameters are given in Table I and the experimental and calculated energy levels are shown in Table II.

## B. Optical absorption and site-selective laser spectroscopy of $\text{Cm}^{3+}/\text{LuPO}_4$

### 1. The intrinsic $\text{Cm}^{3+}$ site

Optical-absorption spectra were obtained for  $\text{Cm}^{3+}$  in  $\text{LuPO}_4$  in the region of 16 000–34 000  $\text{cm}^{-1}$ . Over 70 transitions were observed, of which 60 were assigned to the intrinsic  $D_{2d}$ -symmetry  $\text{Cm}^{3+}$  center (denoted as the A site). Many of the lines were strong, especially in the region from 24 000 to 26 000  $\text{cm}^{-1}$  (see Fig. 4). All of the strong, well-

resolved lines were assigned to the major A site. A number of minor  $\text{Cm}^{3+}$  sites were also present in the  $\text{Cm}^{3+}$ -doped  $\text{LuPO}_4$  crystal. Laser-selective-excitation spectra are presented for the two most prominent minor sites in Fig. 5, and these are compared with the A-site spectrum. Broadband excitation spectra show that almost all of the  $\text{Cm}^{3+}$  ions in this host are located on the A site. This is an expected result since trivalent  $\text{Cm}^{3+}$  ions should readily substitute for  $\text{Lu}^{3+}$  ions in this lattice.

Most of the absorption features of the A site exhibit multi-line structure due to thermal population of all of the nominally  $^8S_{7/2}$ -multiplet crystal-field levels at liquid-helium temperature. The relative change in population of the ground term  $^8S_{7/2}$  doublets as the temperature of the crystal is increased from 6.5 to 29 K is shown in Fig. 6. These doublets were observed previously in EPR experiments by Kot *et al.*,<sup>26</sup> who determined their energies as 0, 3.8, 10.0, 11.6  $\text{cm}^{-1}$ . In this work, site-selective laser spectroscopy permitted a more accurate determination of these levels: 0.00 ( $\Gamma_6$ ), 3.49 ( $\Gamma_7$ ), 8.13 ( $\Gamma_7$ ), and 9.52 ( $\Gamma_6$ )  $\text{cm}^{-1}$ . Polarization experiments confirmed these and other symmetry-group assignments for the A-site doublet levels. In general, the electronic transitions exhibited only very weak polarization behavior.

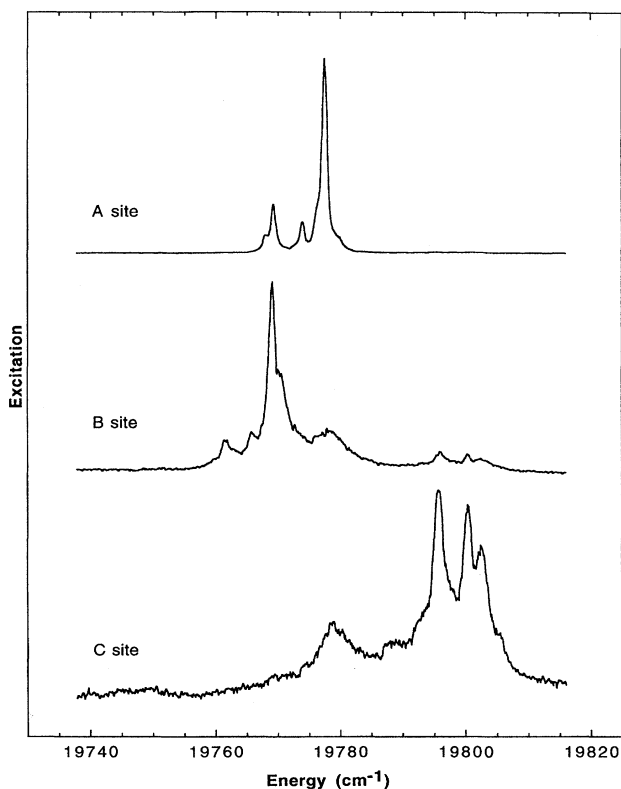


FIG. 5. Site-selective-excitation spectra showing the nominally  $^8S_{7/2}$  to  $^6P_{5/2}$  transitions for  $\text{Cm}^{3+}$  incorporated as a dilute impurity in  $\text{LuPO}_4$ .

TABLE III. Calculated and experimental energy levels for  $\text{Cm}^{3+}/\text{LuPO}_4$  (A site). The numbers before the  $\Gamma_6$  and  $\Gamma_7$  labels in the first column are used to define a particular level and start from the lowest energy level of that irreducible representation.

Level	Largest $^sL_J$ comp.	Calc. energy ( $\text{cm}^{-1}$ )	Expt. energy ( $\text{cm}^{-1}$ )	$E_{\text{exp}} - E_{\text{calc}}$ ( $\text{cm}^{-1}$ )	Level	Largest $^sL_J$ comp.	Calc. energy ( $\text{cm}^{-1}$ )	Expt. energy ( $\text{cm}^{-1}$ )	$E_{\text{exp}} - E_{\text{calc}}$ ( $\text{cm}^{-1}$ )
1 $\Gamma_7$	$^8S_{7/2}$	- .26	0.0	2.6	24 $\Gamma_6$	$^6I_{13/2}$	26 004.5	26 006.0	1.5
1 $\Gamma_6$	$^8S_{7/2}$	0.5	3.49	3.0	25 $\Gamma_7$	$^6D_{9/2}$	26 095.9		
2 $\Gamma_7$	$^8S_{7/2}$	12.1	9.52	-2.6	26 $\Gamma_7$	$^6I_{15/2}$	26 114.2	26 088.0	-26.2
2 $\Gamma_6$	$^8S_{7/2}$	12.8	8.13	-4.7	25 $\Gamma_6$	$^6I_{15/2}$	26 127.2		
3 $\Gamma_7$	$^6D_{7/2}$	16 523.6	16 527.7	4.1	26 $\Gamma_6$	$^6I_{15/2}$	26 232.5		
3 $\Gamma_6$	$^6D_{7/2}$	16 563.2	16 576.7	13.5	27 $\Gamma_7$	$^6I_{15/2}$	26 238.8	26 222.0	-16.8
4 $\Gamma_7$	$^6D_{7/2}$	16 990.4			27 $\Gamma_6$	$^6I_{15/2}$	26 271.1		
4 $\Gamma_6$	$^6D_{7/2}$	17 127.8	17 133.0	5.2	28 $\Gamma_7$	$^6I_{15/2}$	26 312.5	26 273.0	-39.5
5 $\Gamma_6$	$^6P_{5/2}$	19 838.8	19 778.2	-60.5	28 $\Gamma_6$	$^6I_{15/2}$	26 372.8	26 335.0	-37.8
5 $\Gamma_7$	$^6P_{5/2}$	19 993.7	20 017.3	23.7	29 $\Gamma_7$	$^6I_{15/2}$	26 417.3	26 502.0	84.7
6 $\Gamma_6$	$^6P_{5/2}$	20 101.4	20 180.6	79.2	29 $\Gamma_6$	$^6D_{7/2}$	27 866.6	27 888.0	21.4
7 $\Gamma_6$	$^6I_{7/2}$	21 462.4	21 444.3	-18.1	30 $\Gamma_7$	$^6D_{7/2}$	27 910.2	27 910.0	-0.2
6 $\Gamma_7$	$^6I_{7/2}$	21 489.5	21 470.9	-18.6	30 $\Gamma_6$	$^6D_{7/2}$	27 968.0	28 011.0	43.0
8 $\Gamma_6$	$^6I_{7/2}$	21 653.4	21 611.9	-41.5	31 $\Gamma_7$	$^6D_{7/2}$	28 020.8	28 031.0	10.2
7 $\Gamma_7$	$^6I_{7/2}$	21 730.1	21 724.2	-5.9	31 $\Gamma_6$	$^6G_{5/2}$	29 317.0	29 303.4	-13.6
8 $\Gamma_7$	$^6P_{3/2}$	22 062.9	22 035.5	-27.4	32 $\Gamma_7$	$^6G_{5/2}$	29 435.8		
9 $\Gamma_6$	$^6P_{3/2}$	22 165.7	22 135.1	-30.6	32 $\Gamma_6$	$^6G_{5/2}$	29 462.0	29 439.5	-22.5
9 $\Gamma_7$	$^6I_{9/2}$	22 530.6	22 593.3	62.7	33 $\Gamma_7$	$^6D_{1/2}$	29 569.5		
10 $\Gamma_6$	$^6I_{9/2}$	22 687.4	22 673.0	-14.4	33 $\Gamma_6$	$^6I_{7/2}$	29 852.5	29 845.0	-7.5
10 $\Gamma_7$	$^6I_{9/2}$	22 720.4			34 $\Gamma_7$	$^6I_{7/2}$	29 893.2	29 911.0	17.8
11 $\Gamma_7$	$^6I_{9/2}$	22 978.6			35 $\Gamma_7$	$^6I_{7/2}$	29 955.4		
11 $\Gamma_6$	$^6I_{9/2}$	22 988.7	22 948.3	-40.4	34 $\Gamma_6$	$^6I_{7/2}$	30 066.2	30 053.0	-13.2
12 $\Gamma_7$	$^6I_{11/2}$	24 578.2	24 612.0	33.8	35 $\Gamma_6$	$^6D_{5/2}$	30 221.7		
13 $\Gamma_7$	$^6I_{17/2}$	24 696.5	24 693.0	-3.5	36 $\Gamma_6$	$^6D_{5/2}$	30 260.8		
12 $\Gamma_6$	$^6I_{17/2}$	24 706.3	24 726.0	19.7	36 $\Gamma_7$	$^6D_{5/2}$	30 317.9		
14 $\Gamma_7$	$^6I_{17/2}$	24 739.7			37 $\Gamma_7$	$^6D_{3/2}$	30 377.8	30 399.0	21.2
13 $\Gamma_6$	$^6I_{17/2}$	24 763.9	24 794.0	30.1	37 $\Gamma_6$	$^6D_{3/2}$	30 505.7		
15 $\Gamma_7$	$^6I_{17/2}$	24 787.1			38 $\Gamma_6$	$^6G_{11/2}$	30 644.9		
14 $\Gamma_6$	$^6I_{17/2}$	24 844.9	24 834.0	-10.9	38 $\Gamma_7$	$^6G_{11/2}$	30 731.4	30 722.0	-9.4
16 $\Gamma_7$	$^6I_{17/2}$	24 870.2			39 $\Gamma_7$	$^6G_{11/2}$	30 872.9	30 869.0	-3.9
15 $\Gamma_6$	$^6I_{17/2}$	24 875.4	24 877.0	1.6	39 $\Gamma_6$	$^6G_{11/2}$	30 882.1		
17 $\Gamma_7$	$^6I_{17/2}$	24 906.0			40 $\Gamma_7$	$^6G_{11/2}$	31 035.6		
16 $\Gamma_6$	$^6I_{11/2}$	24 927.8			40 $\Gamma_6$	$^6G_{11/2}$	31 146.2		
18 $\Gamma_7$	$^6I_{11/2}$	24 948.8	24 947.0	-1.8	41 $\Gamma_7$	$^6G_{9/2}$	31 673.7		
17 $\Gamma_6$	$^6I_{11/2}$	24 968.7			42 $\Gamma_7$	$^6G_{9/2}$	31 733.2	31 709.0	-24.2
19 $\Gamma_7$	$^6I_{11/2}$	25 090.1	25 102.0	11.9	41 $\Gamma_6$	$^6G_{9/2}$	31 771.6	31 756.0	-15.6
18 $\Gamma_6$	$^6I_{11/2}$	25 173.8			43 $\Gamma_7$	$^6G_{9/2}$	31 790.0		
19 $\Gamma_6$	$^6D_{9/2}$	25 426.1	25 456.0	29.9	42 $\Gamma_6$	$^6G_{9/2}$	31 857.7	31 842.0	-15.7
20 $\Gamma_7$	$^6D_{9/2}$	25 526.5			43 $\Gamma_6$	$^6G_{3/2}$	32 012.3		
20 $\Gamma_6$	$^6I_{13/2}$	25 676.4	25 652.0	-24.4	44 $\Gamma_7$	$^6G_{3/2}$	32 116.0		
21 $\Gamma_7$	$^6D_{9/2}$	25 685.0	25 709.0	24.0	44 $\Gamma_6$	$^6G_{13/2}$	33 596.1	33 598.0	1.9
21 $\Gamma_6$	$^6I_{13/2}$	25 748.7	25 733.0	-15.7	45 $\Gamma_7$	$^6G_{13/2}$	33 661.6	33 640.0	-21.6
22 $\Gamma_7$	$^6I_{13/2}$	25 815.5	25 803.0	-12.5	45 $\Gamma_6$	$^6G_{13/2}$	33 755.2		
22 $\Gamma_6$	$^6I_{13/2}$	25 828.4	25 822.0	-6.4	46 $\Gamma_6$	$^6G_{13/2}$	33 819.0	33 818.0	-1.0
23 $\Gamma_7$	$^6D_{9/2}$	25 858.3	25 866.0	7.7	46 $\Gamma_7$	$^6G_{13/2}$	33 834.3	33 872.0	37.7
23 $\Gamma_6$	$^6I_{13/2}$	25 894.5			47 $\Gamma_7$	$^6G_{13/2}$	33 998.1	34 015.0	16.9
24 $\Gamma_7$	$^6I_{13/2}$	25 951.1							

The experimentally determined *A*-site energy levels are listed in the fourth column of Table III. Again, an initial estimate of the level structure was obtained by substituting the free-ion parameters of  $\text{Cm}^{3+}$  in  $\text{LaCl}_3$  as reported by Carnall<sup>34</sup> and allowing the crystal-field parameters and  $\zeta_f$  to vary. Again the configuration interaction parameters were fixed (except for  $\alpha$  in the final iteration) at their values for  $\text{Cm}^{3+}$  in  $\text{LaCl}_3$ . Comparisons with the experimentally determined levels permitted an identification of most of those levels up to  $25\,000\text{ cm}^{-1}$ . After successive iterations of the fitting process (including varying the free-ion parameters and  $\alpha$ ), 60 levels could be assigned. The final parameters are given in Table I. In several cases the calculated levels vary significantly from the empirical values (by up to  $80\text{ cm}^{-1}$ ). Strong absorption is observed to all of these levels making it unlikely that these features are associated with minor  $\text{Cm}^{3+}$  sites or impurity centers. For this reason, they have been retained in the *A*-site energy scheme.

Excitation of the higher  $\text{Cm}^{3+}$  multiplets, such as  ${}^6P_{5/2}$ , produces fluorescence that appears orange in color; as nonradiative decay processes populate the  ${}^6D_{7/2}$  multiplet.  ${}^6D_{7/2} \rightarrow {}^8S_{7/2}$  fluorescence spectra were obtained for each of the three sites studied. Weak fluorescence originating from the *A*-site  ${}^6P_{5/2}$  multiplet was also observed. The fluores-

cence lifetime of the *A*-site  ${}^6D_{7/2}$  state was measured as  $580 \pm 60\ \mu\text{s}$  and the *A*-site  ${}^6P_{5/2}$  state lifetime was less than 100 ns.

A curious feature of the *A*-site spectrum is the appearance of numerous satellite transitions, both in excitation and fluorescence. In each case, these exhibit common displacements from the four principal transitions associated with the four levels of the ground  ${}^8S_{7/2}$  multiplet. For example, in Fig. 6, satellites are observed  $1.4\text{ cm}^{-1}$  below each excitation transition. Different displacement energies are observed in excitation when monitoring the four distinct fluorescence transitions. Similarly, different displacement energies are observed in fluorescence when pumping the four absorption transitions to each excited level. Both Stokes and anti-Stokes satellite transitions are apparent. These displacements correspond to the specific measured splittings of the nominally  ${}^8S_{7/2}$  ground multiplet. These observations will be discussed in detail elsewhere.

## 2. The minor $\text{Cm}^{3+}$ sites

The *B*-site  ${}^8S_{7/2}$  multiplet levels are located at 0, 1.89, 5.24, and  $9.42\text{ cm}^{-1}$ . Levels of the *B* site are generally lower in energy relative to those of the *A* site (see Table IV). The  ${}^6D_{7/2}$  fluorescence lifetime of  $340 \pm 40\ \mu\text{s}$  is similar to that of the *A* site, and some *B*-site spectra also exhibit satellite transitions.

*C*-site levels are generally displaced to higher energy relative to those of the *A* site. The  ${}^8S_{7/2} \leftrightarrow {}^6D_{7/2}$  transitions are significantly broadened, and it was not possible to determine the  ${}^6D_{7/2}(1)$  level. Excitation transitions to higher multiplets exhibited much narrower linewidths (see Fig. 5), so other levels could be deduced as given in Table IV. The *C*-site fluorescence transitions are sufficiently removed from those of the *A* site to allow good selectivity. However, the fluorescence from the *C* site was too weak to measure any excited-state lifetimes.

## DISCUSSION

The most complete analysis of the optical spectrum of  $\text{Cm}^{3+}$  in a host lattice has been given by Carnall<sup>34</sup> for  $\text{Cm}^{3+}$  diluted in  $\text{LaCl}_3$ . This work was based primarily on data obtained on the isotope  ${}^{244}\text{Cm}$  and published by Gruber *et al.* in 1966.<sup>35</sup> Carnall's analysis assigned 84 levels which were fitted with  $\sigma = 23\text{ cm}^{-1}$ . Carnall found that fitting all the  $F^k$  parameters for  $\text{Cm}^{3+}/\text{LaCl}_3$  resulted in values which were not consistent with the series trend for the  $F^k$  parameters of the trivalent actinide ions in  $\text{LaCl}_3$ . For the final fit Carnall fixed the value of  $F^2$  consistent with the series trend,  $F^4$  and  $F^6$  were freely varied, and constraints were placed on the values of  $\gamma$  and  $T^2$ . For the values of the crystal-field parameters, Carnall found the set derived for  $\text{Bk}^{3+}/\text{LaCl}_3$  fitted as well as allowing the crystal-field parameters for  $\text{Cm}^{3+}/\text{LaCl}_3$  to vary freely, but that using the crystal-field parameters for  $\text{Am}^{3+}/\text{LaCl}_3$  resulted in a poorer fit. Carnall chose to use the  $\text{Bk}^{3+}/\text{LaCl}_3$  crystal-field parameters in the final fit.

Our analysis of  $\text{Cm}^{3+}/\text{LuPO}_4$  fitted 60 levels with a  $\sigma = 30.8\text{ cm}^{-1}$ . As pointed out by Carnall the number of levels measured for  $\text{Cm}^{3+}$  is just a small part of the total

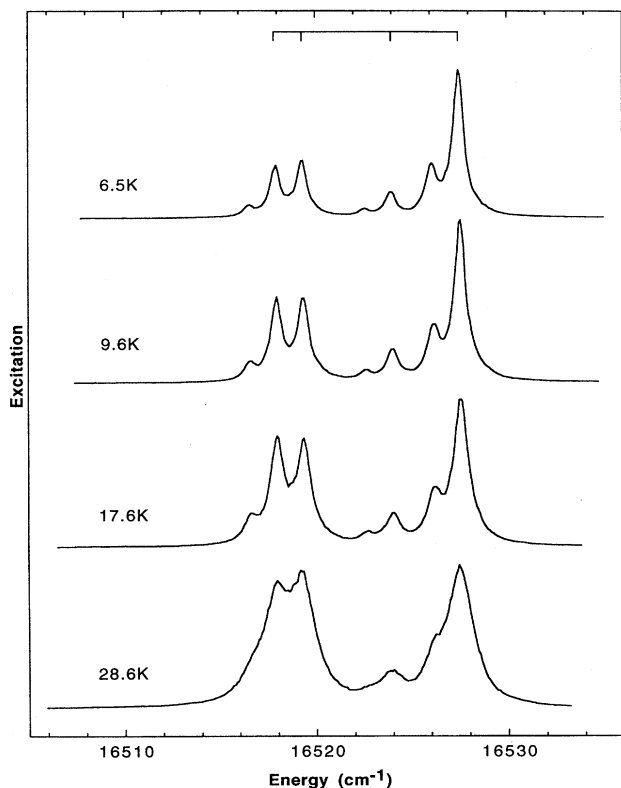


FIG. 6. *A*-site selective-excitation spectra showing the nominally  ${}^8S_{7/2}$  to  ${}^6D_{7/2}$  transitions (indicated) for  $\text{Cm}^{3+}$  incorporated as a dilute impurity in  $\text{LuPO}_4$ . Three distinct satellite transitions are also apparent. This sequence shows how the relative populations of the four nominally  ${}^8S_{7/2}$  crystal-field levels change as the crystal is heated.

TABLE IV. Comparison of the energy levels in sites *A*, *B*, and *C* for  $\text{Cm}^{3+}/\text{LuPO}_4$ . The labels in the first column are taken from Table III for site *A*.

Level	Largest ${}^5L_J$ comp.	Site <i>A</i> ( $\text{cm}^{-1}$ )	Site <i>B</i> ( $\text{cm}^{-1}$ )	Site <i>C</i> ( $\text{cm}^{-1}$ )
$1\Gamma_7$	${}^8S_{7/2}$	0	0	0
$1\Gamma_6$	${}^8S_{7/2}$	3.49	1.89	1.9
$2\Gamma_6$	${}^8S_{7/2}$	8.13	5.24	6.6
$2\Gamma_7$	${}^8S_{7/2}$	9.52	9.42	12.4
$3\Gamma_7$	${}^6D_{7/2}$	16 527.7	16 517.5	
$5\Gamma_6$	${}^6P_{5/2}$	19 778.2	19 771.1	19 800.5
$5\Gamma_7$	${}^6P_{5/2}$	20 017.3	20 007.5	20 037.4

$5f^7$  configuration. In the fitting procedure the  $F^k$ ,  $\alpha$ ,  $\beta$ ,  $\gamma$ , and the crystal-field parameters were allowed to vary freely. In our case we do not have any other analyses of trivalent actinide ions in similar host crystals with which to compare. For  $\text{Gd}^{3+}/\text{LuPO}_4$  the fit used 44 levels and  $\sigma = 15.5 \text{ cm}^{-1}$  was obtained with a similarly limited number of experimental levels. The values of the crystal-field parameters for  $\text{Gd}^{3+}/\text{LuPO}_4$  may be compared with the values for other trivalent rare-earth ions in this host crystal as tabulated by Williams.<sup>36</sup> All the parameters fall within the range found for the other trivalent ions except for  $B_4^6$ , which is appreciably larger than the other values. Although the error in this parameter was found to be less than 10% of its value,  $B_4^6$  is probably not well determined as it mixes the same states as  $B_4^4$  and the number of levels measured is limited. The ratio of  $N'_v$  for  $\text{Cm}^{3+}/\text{LuPO}_4$  to  $\text{Gd}^{3+}/\text{LuPO}_4$  (see Table I) is approximately 2, which is consistent with an earlier study of  $\text{Cm}^{3+}(\text{Gd}^{3+})/\text{ThO}_2$  and other isoelectronic trivalent actinide/lanthanide comparisons.<sup>37,38</sup>

The splitting of the nominally  ${}^8S_{7/2}$  ground term has been the focus of earlier studies using the EPR technique.<sup>26</sup> It now appears that the analysis of this data yielded a total ground-term crystal-field splitting which was too large. However, it should be noted that the splittings between the pairs of close-lying doublets  $1\Gamma_7$ ,  $1\Gamma_6$  and  $2\Gamma_6$ ,  $2\Gamma_7$  (notation of Table III) were 3.8 and  $1.4 \text{ cm}^{-1}$ , respectively, from the EPR analysis, which are in good agreement with the optical splittings given in Table III. The major inaccuracy in the EPR results arises in the differences between the two sets of doublets (the  $1\Gamma_6 - 2\Gamma_6$  difference) which was found to be  $6.2 \text{ cm}^{-1}$  from the EPR measurements, and is  $4.6 \text{ cm}^{-1}$  from the optical data. The calculated energies of the ground term are of the right magnitude with two pairs of close-lying doublets separated by approximately  $11 \text{ cm}^{-1}$ . The calculated levels are in the correct order except that  $2\Gamma_6$  and  $2\Gamma_7$  are interchanged. This is a consequence of the rather small splittings and the general quality of the fit which has  $\sigma = 30.8 \text{ cm}^{-1}$ . A somewhat similar problem was encountered in ground-state splittings of  $\text{Cm}^{3+}/\text{LaCl}_3$ ,<sup>39</sup> where the EPR data and the optical data appeared to be in conflict, but subsequent high-resolution optical measurements resolved the discrepancies. In the  $\text{Cm}^{3+}/\text{ThO}_2$  system the crystal field is large enough so that the parameters of the optical analysis reproduce the ground-term splittings rather well.<sup>37</sup>

The wave functions obtained from the final diagonalization of the Hamiltonian matrices can be used to calculate the

TABLE V. Comparison of the calculated and measured  $g$  values for the nominally  ${}^8S_{7/2}$  ground term of  $\text{Cm}^{3+}/\text{LuPO}_4$ .

Energy level	$g_{\parallel}(\text{cal})$	$g_{\parallel}(\text{exp})^a$	$g_{\perp}(\text{cal})$	$g_{\perp}(\text{exp})^a$
$1\Gamma_7$	12.29	(12.69) <sup>b</sup>	0.61	(0.25) <sup>b</sup>
$1\Gamma_6$	7.50	7.977(5)	4.64	4.102(2)
$2\Gamma_6$	3.64	4.12(1)	4.64	4.10(1)
$2\Gamma_7$	0.70	1.380	7.11	7.284(10)

<sup>a</sup>Reference 26.

<sup>b</sup>Calculated in Ref. 26 using a free-ion  $g$  value of 1.925.

$g$  values for the crystal-field states of the ground multiplet and these can be compared with those obtained from EPR spectroscopy. This comparison is shown in Table V. The trend in the calculated  $g$  values follows the experimental values. However, the fact that in one case the difference between  $g(\text{exp})$  and  $g(\text{cal})$  is as much as 0.7 suggests the error in the energies (or crystal-field parameters for the ground term) is enough to affect the calculated  $g$  values. This is not surprising as the calculation of the Zeeman splittings or  $g$  values is a much more severe test of the wave functions than the energy differences.<sup>40</sup> Undoubtedly just obtaining the crystal-field parameters for the ground term only would result in much better agreement between the calculated and experimental energies and calculated and experimental  $g$  values. Essentially this was done for  $\text{Cm}^{3+}/\text{LuPO}_4$  in the earlier EPR paper<sup>26</sup> and for the energy levels of  $\text{Cm}^{3+}/\text{LaCl}_3$ .<sup>39</sup>

## CONCLUSION

Optical-absorption and laser-selective-excitation techniques have been used to obtain spectra of the  $5f^7$  ion  $\text{Cm}^{3+}$  in  $\text{LuPO}_4$ . Three distinct  $\text{Cm}^{3+}$  sites were found, the principal site being the  $D_{2d}$ -symmetry substitutional site. High-resolution spectra were used to refine the values of the nominally  ${}^8S_{7/2}$  ground-term splittings and these were compared with earlier EPR results. Excited energy levels up to  $35\,000 \text{ cm}^{-1}$  were observed and analyzed using a least-squares fitting procedure. This is the most complete optical study and crystal-field analysis reported for a trivalent actinide in the  $\text{LuPO}_4$  host crystal.

One-photon absorption and excitation spectra were also obtained for the  $4f^7$  ion  $\text{Gd}^{3+}$  in  $\text{LuPO}_4$ . Two-photon excitation was also observed to the  ${}^6P_{7/2}$  and  ${}^6P_{5/2}$  multiplets and the energy levels were determined for the  $D_{2d}$  symmetry site up to  $37\,000 \text{ cm}^{-1}$ . A similar fitting procedure as for  $\text{Cm}^{3+}$  was performed for  $\text{Gd}^{3+}$  and the two systems were compared.

Satellite transitions have been observed in both the fluorescence and excitation spectra of the  $\text{Cm}^{3+}/\text{LuPO}_4$  crystal. These phenomena will be the subject of a future communication.

## ACKNOWLEDGMENTS

This research was sponsored by the Division of Material Sciences, U.S. Department of Energy under Contract No. DE-AC05-84OR21400 with Martin Marietta Energy Systems, Inc., and by the Director, Office of Energy Research,

Office of Basic Energy Sciences, Chemical Sciences Division of the U.S. Department of Energy under Contract No. DE-AC03-76SF00098. The authors are indebted for the use of the  $^{248}\text{Cm}$  to the Division of Chemical Sciences, Office of

Basic Energy Sciences, through the transplutonium element production facilities at Oak Ridge National Laboratory. The authors also acknowledge with thanks the excellent technical contributions of H. E. Harmon and C. B. Finch.

- <sup>1</sup>D. F. Mullica, W. O. Milligan, D. A. Grossie, G. W. Beall, and L. A. Boatner, *Inorg. Chim. Acta* **95**, 231 (1984).
- <sup>2</sup>D. F. Mullica, D. A. Grossie, and L. A. Boatner, *J. Solid State Chem.* **58**, 71 (1985).
- <sup>3</sup>L. A. Boatner and B. C. Sales, in *Radioactive Waste Forms for the Future*, edited by W. Lutze and R. C. Ewing (North-Holland, Amsterdam, 1988), p. 495.
- <sup>4</sup>B. C. Sales, C. W. White, and L. A. Boatner, *Nucl. Chem. Waste Manage.* **4**, 281 (1983).
- <sup>5</sup>L. A. Boatner, M. M. Abraham, and B. C. Sales, *Inorg. Chim. Acta* **94**, 146 (1983).
- <sup>6</sup>M. M. Abraham, L. A. Boatner, T. C. Quinby, D. K. Thomas, and M. Rappaz, *Radioactive Waste Manage.* **1**, 181 (1980).
- <sup>7</sup>B. C. Sales, M. Petek, and L. A. Boatner, in *Scientific Basis for Nuclear Waste Management VI*, edited by D. G. Brookins (North-Holland, Amsterdam, 1983), Vol. 15, p. 251.
- <sup>8</sup>L. A. Boatner, M. M. Abraham, and M. Rappaz, in *Scientific Basis for Nuclear Waste Management*, edited by J. G. Moore (Plenum, New York, 1981), Vol. 3, p. 181.
- <sup>9</sup>L. Cartz, F. G. Karioris, R. A. Fournelle, and K. A. Gowda, *Radiat. Eff. Lett.* **67**, 83 (1981).
- <sup>10</sup>R. C. Ewing, *Am. Mineral.* **60**, 728 (1975).
- <sup>11</sup>C. W. Bjorkland, *J. Am. Chem. Soc.* **79**, 6347 (1958).
- <sup>12</sup>C. Keller and K. H. Walter, *Inorg. Nucl. Chem.* **27**, 1253 (1965).
- <sup>13</sup>S. W. Allison, G. T. Gillies, and L. A. Boatner, *Appl. Opt.* (to be published).
- <sup>14</sup>A. Lempicki, E. Berman, A. J. Wojtowicz, M. Balcerzyk, and L. A. Boatner, *IEEE Trans. Nucl. Sci.* **40**, 384 (1993).
- <sup>15</sup>P. C. Becker, T. Hayhurst, G. Shalimoff, J. G. Conway, N. Edelstein, L. A. Boatner, and M. M. Abraham, *J. Chem. Phys.* **81**, 2872 (1984).
- <sup>16</sup>J. Sytsma, D. Piehler, N. M. Edelstein, L. A. Boatner, and M. M. Abraham, *Phys. Rev. B* **47**, 14 786 (1993).
- <sup>17</sup>T. Hayhurst, G. Shalimoff, J. G. Conway, N. Edelstein, L. A. Boatner, and M. M. Abraham, *J. Chem. Phys.* **76**, 3960 (1982).
- <sup>18</sup>M. Rappaz, L. A. Boatner, and M. M. Abraham, *J. Chem. Phys.* **73**, 1095 (1980).
- <sup>19</sup>M. M. Abraham, L. A. Boatner, J. O. Ramey, and M. Rappaz, *J. Chem. Phys.* **78**, 3 (1983).
- <sup>20</sup>C.-K. Loong, L. Soderholm, M. M. Abraham, L. A. Boatner, and N. M. Edelstein, *J. Chem. Phys.* **98**, 4214 (1993).
- <sup>21</sup>C.-K. Loong, L. Soderholm, J. P. Hammonds, M. M. Abraham, L. A. Boatner, and N. M. Edelstein, *J. Phys. Condens. Matter* **5**, 5121 (1993).
- <sup>22</sup>G. M. Williams, P. C. Becker, J. G. Conway, N. Edelstein, L. A. Boatner, and M. M. Abraham, *Phys. Rev. B* **40**, 4132 (1989).
- <sup>23</sup>P. C. Becker, N. Edelstein, G. M. Williams, J. J. Bucher, R. E. Russo, J. A. Koningstein, L. A. Boatner, and M. M. Abraham, *Phys. Rev. B* **31**, 8102 (1985).
- <sup>24</sup>M. M. Abraham and L. A. Boatner, *Phys. Rev. B* **26**, 1434 (1982).
- <sup>25</sup>M. M. Abraham, L. A. Boatner, C. B. Finch, W. K. Kot, J. G. Conway, G. V. Shalimoff, and N. M. Edelstein, *Phys. Rev. B* **35**, 3057 (1987).
- <sup>26</sup>W. K. Kot, N. M. Edelstein, M. M. Abraham, and L. A. Boatner, *Phys. Rev. B* **48**, 12 704 (1993).
- <sup>27</sup>L. A. Boatner, G. W. Beall, M. M. Abraham, C. B. Finch, R. J. Floran, P. G. Huray, and M. Rappaz, in *Management of Alpha Contaminated Wastes* (International Atomic Energy Agency, Vienna, 1981), p. 114.
- <sup>28</sup>M. Rappaz, L. A. Boatner, and M. M. Abraham, *J. Chem. Phys.* **73**, 1045 (1980).
- <sup>29</sup>G. F. Koster, J. O. Dimmock, R. G. Wheeler, and H. Statz, *Properties of the Thirty-Two Point Groups* (MIT, Cambridge, MA, 1963).
- <sup>30</sup>W. T. Carnall, H. Crosswhite, H. M. Crosswhite, J. P. Hessler, N. M. Edelstein, J. G. Conway, G. V. Shalimoff, and R. Sarup, *J. Chem. Phys.* **72**, 5089 (1980).
- <sup>31</sup>B. G. Wybourne, *Spectroscopic Properties of Rare Earths* (Wiley, New York, 1963).
- <sup>32</sup>F. Auzel and O. L. Malta, *J. Phys.* **44**, 201 (1983).
- <sup>33</sup>W. T. Carnall, G. L. Goodman, K. Rajhak, and R. S. Rana, *J. Chem. Phys.* **90**, 3443 (1989).
- <sup>34</sup>W. T. Carnall, *J. Chem. Phys.* **96**, 8713 (1992).
- <sup>35</sup>J. B. Gruber, W. R. Cochran, J. G. Conway, and A. T. Nicol, *J. Chem. Phys.* **45**, 1423 (1966).
- <sup>36</sup>G. M. Williams, Ph.D. thesis, UC Berkeley, 1988.
- <sup>37</sup>P. Thouvenot, S. Hubert, and N. Edelstein, *Phys. Rev. B* **50**, 9715 (1994).
- <sup>38</sup>N. M. Edelstein, *J. Alloys Compounds* **223**, 197 (1995).
- <sup>39</sup>G. K. Liu, J. V. Beitz, and J. Huang, *J. Chem. Phys.* **99**, 3304 (1993).
- <sup>40</sup>H. M. Crosswhite, H. Crosswhite, W. T. Carnall, and A. P. Paszek, *J. Chem. Phys.* **72**, 5103 (1980).